

INTELLIGENT SYSTEMS MODEL FOR SELECTIVE LASER MELTING (SLM) ADDITIVE MODELING OF THE DAMPING OF TI-6AL-4V IN TURBULENT FLOW DURING POWDER BED MELTING IN THE MANUFACTURING PROCESS

R. Belgada*

(LARILE) Laboratory of Advanced Research on Industrial and Logistics Engineering,
ENSEM, Hassan II University of Casablanca, MOROCCO
E-mail: belgada.rihab@gmail.com

A. Mzerd

(SSTE) Faculty of Science, Mohammed V University, Department of Physic,
Mechanical Engineering, Rabat, MOROCCO

With industrial modernity and its multiple advantages over global industry. The use of 3D printers has become a primary necessity for the industry. The laser melting process (SLM) is one of the most widely used processes for the manufacture of metal parts from a powder. Thanks to laser fusion manufacturing, very complex structures and geometries can be produced with very good quality. The materials used in SLM are metals that come in the form of granules. During the manufacture of the parts, the metal powder cannot be compacted as much during the process. It is therefore necessary to use supports for cantilevered structures. The interest of our research is to model the suspension mechanism of Ti-6Al-4v granules in a turbulent flow of Newtonian fluid due to the fusion of granules in a powder bed. We will start with a mathematical study based on the transport equation for Ti-6Al-4v granules and the Navier-Stokes equations. Then the mathematical and numerical discretization of the equations is done by using the method of finite volume, for the resolution of the equations we use the Gauss-Seidel method. And finally, we built a numerical code for the resolution of the fluid velocity equations and the concentration profile of the granules in the FORTRAN language.

Key words: Additive manufacturing, Ti-6Al-4v transport, Selective laser melting, Suspension of Ti-6Al-4v granules.

1. Introduction

Many physical phenomena such as metal melting and evaporation, particle projection, solidification, ...and significant thermal cycles occur during the SLM process as a result of the input of energy from the laser. These phenomena depend on the operating parameters used and some can affect the quality of the product obtained. The mastery of the SLM process generally involves a heavy experimental phase. Numerical modelling represents an alternative and makes it possible to predict the laser-target interaction by considering the environment in the process. The interest of our research is to model the suspension mechanism of Ti-6Al-4v granules in a turbulent flow of Newtonian fluid due to the fusion of granules in a powder bed [1],[2],[4],[5].

The mechanism of very fast total melting/solidification of metal in the SLM process promotes the properties of the products produced. This results in a higher quality of microstructure, better finish and higher density compared to processes Sintering (SLS). The SLM process has many input parameters that are summarized as follows:

* To whom correspondence should be addressed

Laser beam parameter

- ✓ Laser power
- ✓ Beam diameter
- ✓ Wavelength
- ✓ Continuous or pulsed mode

Material parameter

- ✓ Chemical composition
- ✓ Particle size
- ✓ Form of the powder
- ✓ Flowability
- ✓ Physical properties
- ✓ Density

Machine parameter

- ✓ Room temperature
- ✓ Laser speed
- ✓ Trajectory of the laser
- ✓ Layer height
- ✓ Gas in the room
- ✓ Deviation between vectors
- ✓ Vector length

Part parameter

- ✓ Room height
- ✓ Function

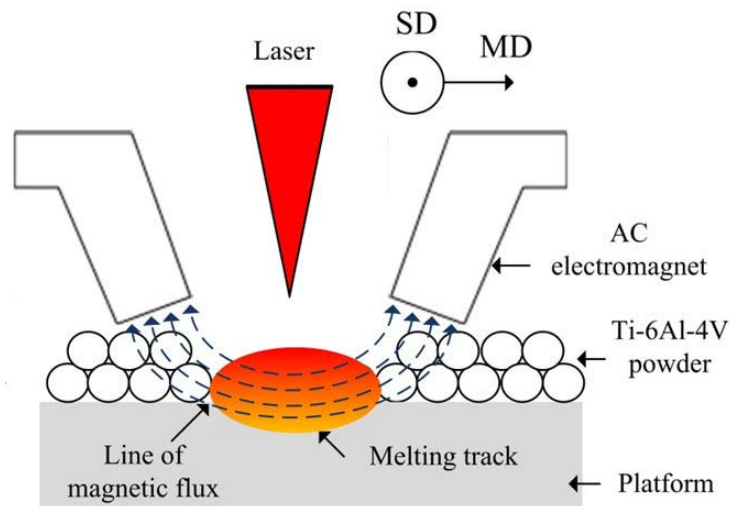


Fig.1. Simplified diagram of the selective laser fusion manufacturing process of a powder bed of Ti-6Al-4V.

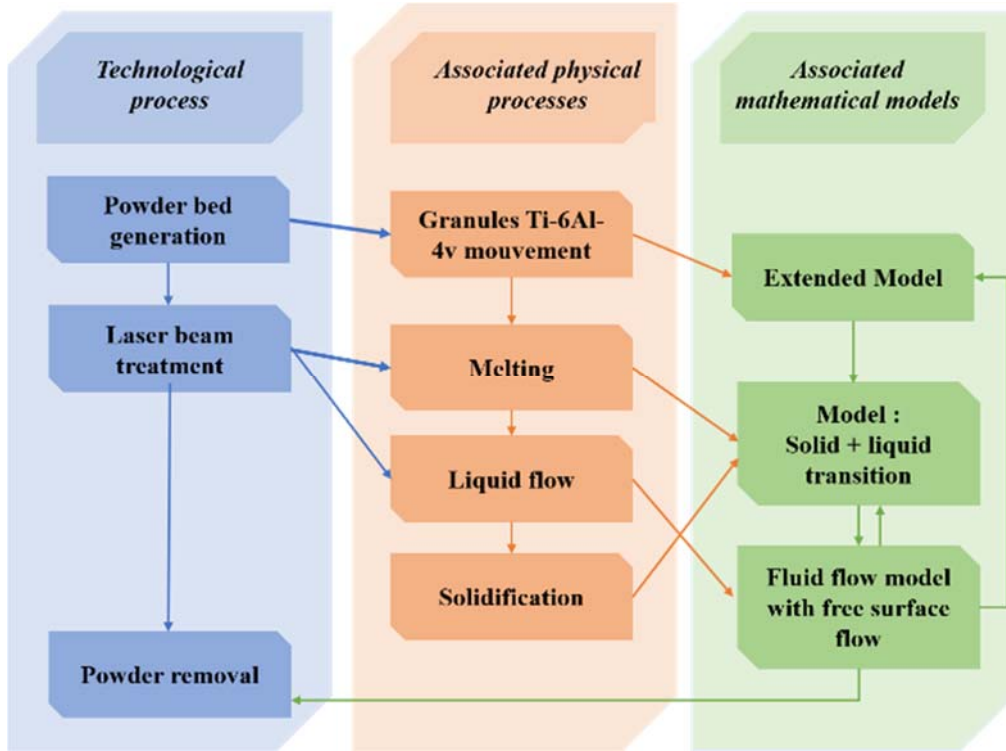


Fig.2. Diagram of SLM technological process.

Research [19], [20], [21] has investigated the influence of operating parameters and have shown that it is the power of the laser and the scanning speed of the beam that determine the thermal history during manufacturing and therefore the quality of the parts obtained.

2. Mathematical modeling

2.1. Quantity of motion equation

The Navier-Stokes momentum conservation equation:

$$\frac{\partial \vec{U}}{\partial t} + \vec{U} \text{grad}(\vec{U}) = \frac{-1}{\rho} \text{grad}(\vec{P}) + \nu \psi \vec{U} + \vec{g}. \tag{2.1}$$

In Cartesian coordinates, Eq.(2.1) is written:

$$\frac{\partial \alpha}{\partial t} + \frac{\partial(\alpha\alpha)}{\partial x} + \frac{\partial(\alpha\beta)}{\partial z} = \frac{-1}{\rho} \frac{\partial P}{\partial x} + \nu \left(\frac{\partial^2 \alpha}{\partial x^2} + \frac{\partial^2 \beta}{\partial z^2} \right), \tag{2.2}$$

and

$$\frac{\partial \alpha}{\partial t} + \frac{\partial(\beta\alpha)}{\partial x} + \frac{\partial(\beta\beta)}{\partial z} = \frac{-1}{\rho} \frac{\partial P}{\partial z} + \nu \left(\frac{\partial^2 \alpha}{\partial x^2} + \frac{\partial^2 \beta}{\partial z^2} \right) + \vec{g}. \tag{2.3}$$

2.2. Transport equation

The transport equation for the concentration of granules in an air flow will be written in the following form [6], [13]:

$$\frac{\partial C_g}{\partial t} + (\bar{U} \bar{\nabla} C_g) = M_m \psi C_g. \quad (2.4)$$

This equation can be written as follows in two dimensions (x, z):

$$\frac{\partial C_g}{\partial t} + \frac{\partial (C_g \alpha)}{\partial x} + \frac{\partial (C_g \beta)}{\partial z} = M_m \left(\frac{\partial^2 C_g}{\partial x^2} + \frac{\partial^2 C_g}{\partial z^2} \right). \quad (2.5)$$

2.3. Continuity equation

The continuity equation in the case of incompressible flows then reduces to:

$$\text{div}(\bar{U}) = 0, \quad (2.6)$$

where $\bar{U} = \alpha \bar{e}_x + \beta \bar{e}_z$ is the field of airflow velocity, (\bar{e}_x, \bar{e}_z) the Cartesian system, can be written the Eq.(2.1) in two dimensions as follows:

$$\frac{\partial \alpha}{\partial x} + \frac{\partial \beta}{\partial z} = 0. \quad (2.7)$$

3. Experimental study

We did an analysis for the sample studied on the scanning electron microscope and an energy dispersive X-ray spectroscopy in our laboratory to find out the morphology as well as the chemical properties of the sample.

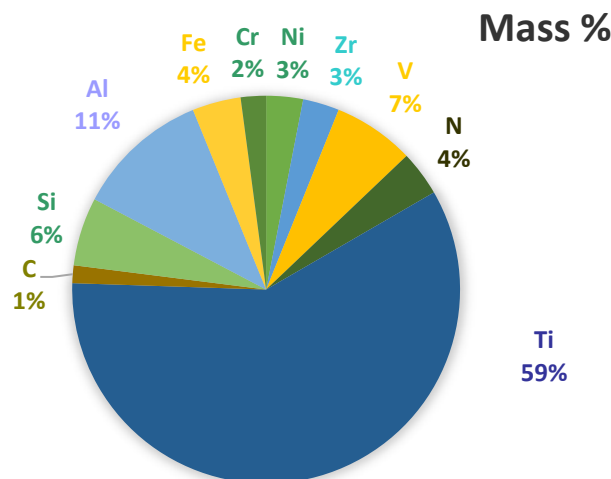


Fig.3. The mass of the chemical components of Ti-6Al-4v by energy-dispersive X-ray spectroscopy EDXS.

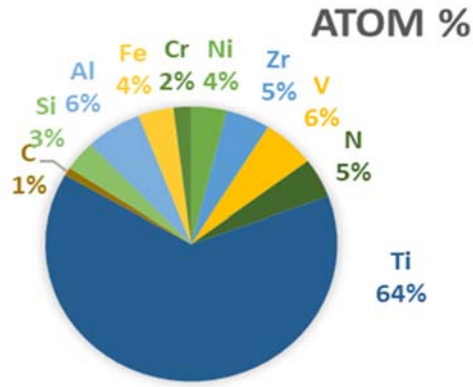


Fig.4. Atomic composition of the chemical components of Ti-6Al-4v by energy-dispersive X-ray spectroscopy EDXS.



Fig.5. Sample preparation TI-6al-4v in JOEL-JFC.



Fig.6. SLM machine EOSINT M270.

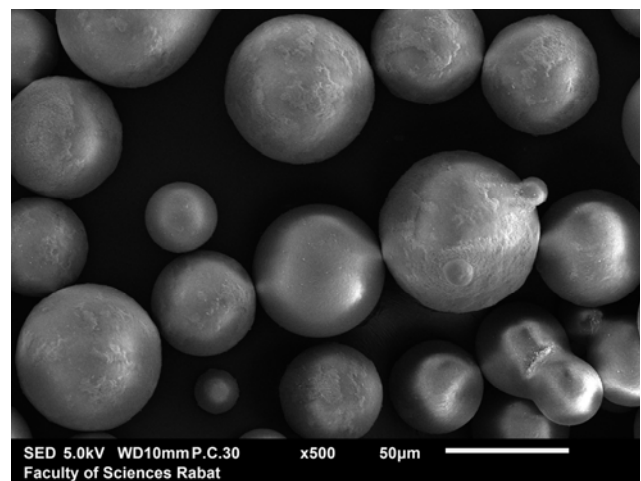
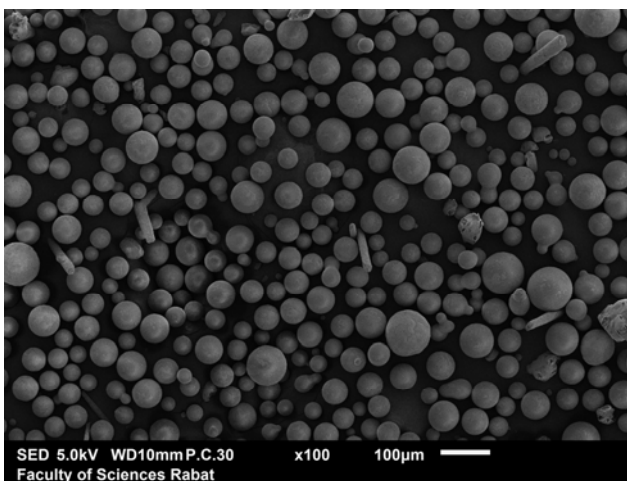


Fig.7. Ti-6Al-4v granule in scanning electron microscope (SEM)×100 and ×500 .

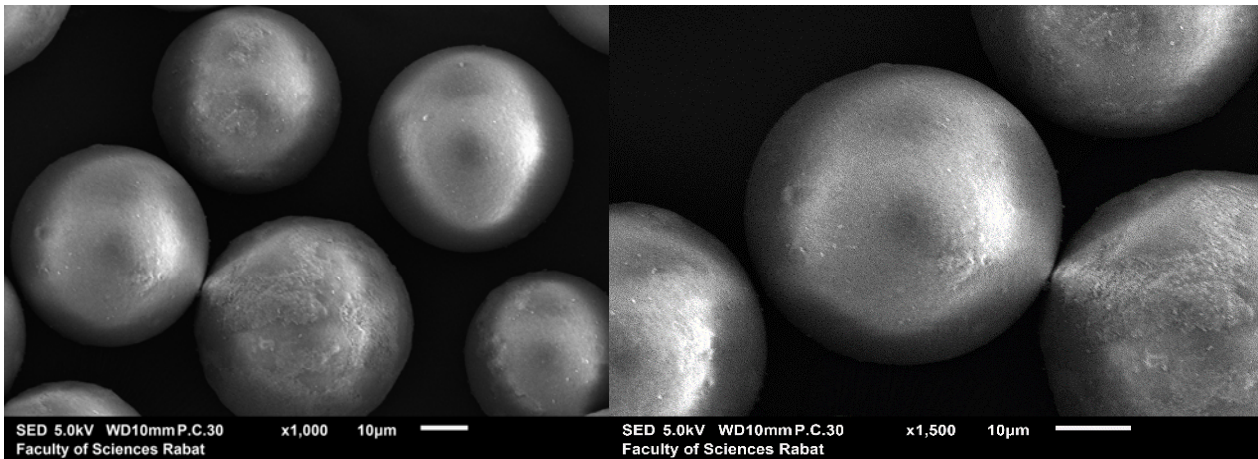


Fig.9 and 10. Ti-6Al-4v granule in scanning electron microscope (SEM)×1000 and ×5000 .

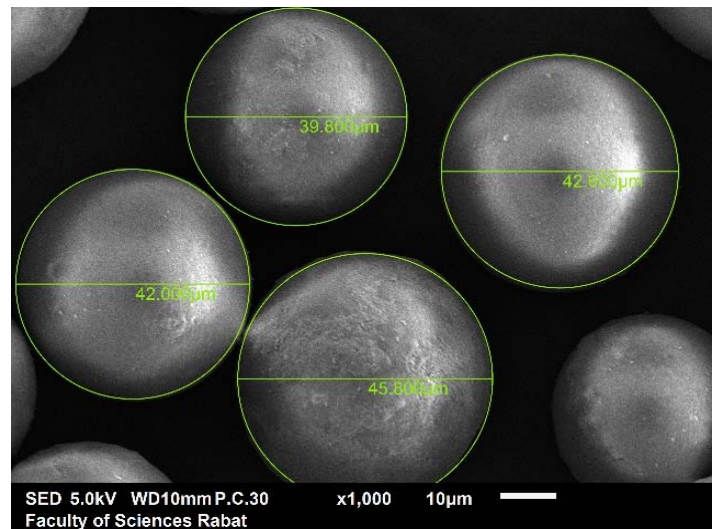


Fig.11. Diameters of Ti-6Al-4v granule in scanning electron microscope (SEM)×1000 .

Figures 7-11 show the geometric morphology of ti-6Al-4v granules and the texture and shape of the granules on scanning electron microscopy (SEM). The machine is equipped with a maximum power ytterbium fiber laser limited to 120 W . The diameter of the laser beam is $34\ \mu\text{m}$. The machine has a manufactured in dimensions $250, 250, 300\ \text{mm}^3$ (X, Y, Z). The z -axis is expandable to a maximum depth of $360\ \text{mm}$.

The powder feeding system consists of a drum driven by a motor, he deposits a quantity of powder on the tray, then a scraper spreads the powder on its return. The thickness of the powder layer to be deposited is adjustable according to the height at which the production plate is lowered along the z -axis of the machine.

4. Average equations and fluctuations

The Reynolds decomposition to all the following equations and relations reflects the decomposition, at a given time:

$$\alpha = \bar{\alpha} + \alpha', \quad (4.1)$$

$$\beta = \bar{\beta} + \beta', \quad (4.2)$$

$$P = \bar{P} + P', \quad (4.3)$$

$$C_g = \bar{C}_g + C_g', \quad (4.4)$$

where: α' , β' , P' and C_g' the fluctuation components, $\bar{\alpha}$, $\bar{\beta}$, \bar{P} and \bar{C}_g the averaged components.

4.1. Quantity of motion equation

We introduce the decomposition of Reynolds on the continuity Eq.(2.1) it becomes:

$$\frac{\partial \bar{\alpha}_i}{\partial t} + \bar{\alpha}_j \frac{\partial (\bar{\alpha}_i)}{\partial x_j} = \frac{-I \partial \bar{P}}{\rho \partial x_i} + \frac{I}{\rho} \frac{\partial}{\partial x_j} \left(\mu_M \left(\frac{\partial \bar{\alpha}_i}{\partial x_j} + \frac{\partial \bar{\alpha}_j}{\partial x_i} \right) - \overline{\rho \alpha'_i \alpha'_j} \right) + g_i. \quad (4.5)$$

In the direction \bar{e}_x :

$$\frac{\partial \bar{\alpha}}{\partial t} + \frac{\partial (\bar{\alpha} \bar{\alpha})}{\partial x} + \frac{\partial (\bar{\alpha} \bar{\beta})}{\partial z} = \frac{-I \partial \bar{P}}{\rho \partial x} + \frac{I}{\rho} \left\{ \mu_M \left(\frac{\partial^2 \bar{\alpha}}{\partial x^2} + \frac{\partial^2 \bar{\beta}}{\partial z^2} \right) + \left[\frac{\partial}{\partial x} (-\overline{\rho \alpha' \alpha'}) + \frac{\partial}{\partial z} (-\overline{\rho \alpha' \beta'}) \right] \right\}. \quad (4.6)$$

In the direction \bar{e}_z :

$$\frac{\partial \bar{\beta}}{\partial t} + \frac{\partial (\bar{\beta} \bar{\alpha})}{\partial x} + \frac{\partial (\bar{\beta} \bar{\beta})}{\partial z} = \frac{-I \partial \bar{P}}{\rho \partial y} + \frac{I}{\rho} \left\{ \mu_M \left(\frac{\partial^2 \bar{\alpha}}{\partial x^2} + \frac{\partial^2 \bar{\beta}}{\partial z^2} \right) + \left[\frac{\partial}{\partial x} (-\overline{\rho \alpha' \beta'}) + \frac{\partial}{\partial z} (-\overline{\rho \beta' \beta'}) \right] \right\} - g. \quad (4.7)$$

We take, $R_{ij} = -\overline{\rho \alpha'_i \alpha'_j}$ the Reynolds tensor.

4.2. Transport equation

It's the same study, for the quantity of motion equation we obtain:

$$\frac{\partial \bar{C}_g}{\partial t} + \frac{\partial (\bar{C}_g \bar{\alpha})}{\partial x} + \frac{\partial (\bar{C}_g \bar{\beta})}{\partial z} = M_m \left(\frac{\partial^2 \bar{C}_g}{\partial x^2} + \frac{\partial^2 \bar{C}_g}{\partial z^2} \right) - \frac{\partial \overline{\rho \alpha' C'_g}}{\partial x} - \frac{\partial \overline{\rho \beta' C'_g}}{\partial z}. \quad (4.8)$$

The amount of mass of turbulent flows in the vertical and horizontal directions: $(-\overline{\rho \beta' C'_g})$ and $(-\overline{\rho \alpha' C'_g})$. It introduces in Eqs (4.6), (4.7) and (4.8) five new variables: Reynolds' normal stresses: $(-\overline{\rho \alpha' \alpha'})$ and $(-\overline{\rho \beta' \beta'})$ shear stress of Reynolds $(-\overline{\rho \alpha' \beta'})$.

4.3. Continuity equation

Similarly, for the quantity of motion equation we obtain:

$$\frac{\partial \bar{\alpha}}{\partial x} + \frac{\partial \bar{\beta}}{\partial z} = 0. \quad (4.9)$$

4.3. Continuity equation

Similarly, for the quantity of motion equation we obtain:

$$\frac{\partial \bar{\alpha}}{\partial x} + \frac{\partial \bar{\beta}}{\partial z} = 0. \quad (4.10)$$

4.4. Turbulence model

The number of equations is smaller than the number of unknowns. The main interest of turbulence flow models is to have an estimate of these terms. By reducing the number of unknowns in the new equations [7], [8], [9]. Reynolds as a function of dynamic viscosity and average strain rate:

$$-\rho \overline{\alpha'_i \alpha'_j} = \mu_t \left(\frac{\partial \bar{\alpha}_i}{\partial x_j} + \frac{\partial \bar{\alpha}_j}{\partial x_i} \right). \quad (4.11)$$

The concentration fluxes of the granules $(-\rho \overline{\alpha'_i C'_g})$, $(-\rho \overline{\beta'_i C'_g})$ are solved with the same method as the Reynolds tensor. The turbulent flow viscosity can be defined by the following relation of the model $\kappa_t - \kappa_r$:

$$\nu = C_{g\mu_m} \frac{\kappa_t}{\kappa_r}, \quad (4.12)$$

where, $C_{g\mu_m}$: semi-empirical coefficient 0.095, κ_t : the dissipation of turbulent energy, κ_r : turbulent flow kinetic energy, $\tau_{C'_g}$: coefficient of concentration distribution granules, δ_e : number of turbulent Schmidt. The equation becomes:

$$-\rho \overline{C'_g \alpha'_i} = \tau_{C'_g} \frac{\partial \bar{C}_g}{\partial x_i} = \frac{\mu_t}{\delta_e} \frac{\partial \bar{C}_g}{\partial x_i}. \quad (4.13)$$

With κ_t et κ_r the equation become:

$$\frac{\partial(\rho \kappa_t)}{\partial t} + \frac{\partial(\rho \kappa_t \bar{\alpha})}{\partial x} + \frac{\partial(\rho \kappa_t \bar{\beta})}{\partial z} = \frac{\partial}{\partial x} \left[\left(\frac{\mu_t}{\delta_\kappa} \frac{\partial \kappa_t}{\partial x} \right) + \left(\frac{\mu_t}{\delta_\kappa} \frac{\partial \kappa_t}{\partial z} \right) \right] + V + W - \rho \kappa_r \quad (4.14)$$

and

$$\frac{\partial(\rho \kappa_r)}{\partial t} + \frac{\partial(\rho \kappa_r \bar{\alpha})}{\partial x} + \frac{\partial(\rho \kappa_r \bar{\beta})}{\partial z} = \frac{\partial}{\partial x} \left[\left(\frac{\mu_t}{\delta_\kappa} \frac{\partial \kappa_r}{\partial x} \right) + \left(\frac{\mu_t}{\delta_\kappa} \frac{\partial \kappa_r}{\partial z} \right) \right] - C_{g\kappa_2} \frac{\kappa_r^2}{\kappa_t} + C_{g\kappa_1} \frac{\kappa_r}{\kappa_t} (V + C_{g\kappa_3} W), \quad (4.15)$$

where
$$V = -\overline{\rho\alpha'_i\alpha'_j} \frac{\partial\overline{\alpha}_i}{\partial x_j} = \mu_t \frac{\partial\overline{\alpha}_i}{\partial x_j} \left(\frac{\partial\overline{\alpha}_i}{\partial x_j} + \frac{\partial\overline{\alpha}_j}{\partial x_i} \right). \tag{4.16}$$

V is the kinetic energy production of turbulent flow in reaction with turbulent stress vectors and velocity gradients

and
$$W = \rho\epsilon g_i \overline{c_i\alpha'_j} \tag{4.17}$$

The constants are deduced from the results of simple experiments and are all borrowed $C_{g\kappa_3}$ since they are not concerned with the effects of buoyancy [10-12].

$$\delta_{\kappa_t} = 2.0, \tag{4.18}$$

$$\delta_{\kappa_r} = 2.3, \tag{4.19}$$

$$\delta_{I\kappa_r} = 2.44, \tag{4.20}$$

$$C_{g\kappa_{r2}} = 2.92. \tag{4.21}$$

For $C_{g\kappa_3}$: $C_{g\kappa_3} = 0$. Stable laminar flow of directions $F < 0$, $C_{g\kappa_3} = 1$. Unstable laminar flow of directions $F > 0$.

5. Results and discussions

After presenting all the conceptual, mathematical and numerical bases in. the objective of this study phase is to present the results obtained by the code established in FORTRAN.

The calculations are initiated by an initial profile, which can be absolutely indescribable as long as it satisfies the boundary conditions. However, to reduce the computation time, a profile of a Newtonian fluid in a flat surface pipe with a continuous turbulent flow is used, the turbulence model used is the $\kappa_t - \kappa_r$:

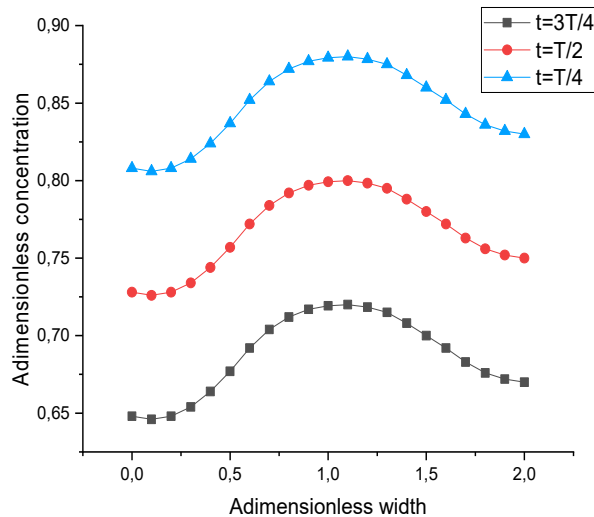


Fig.14. Dimensionless granule Ti-6Al-4v concentration as a function of dimensionless width.

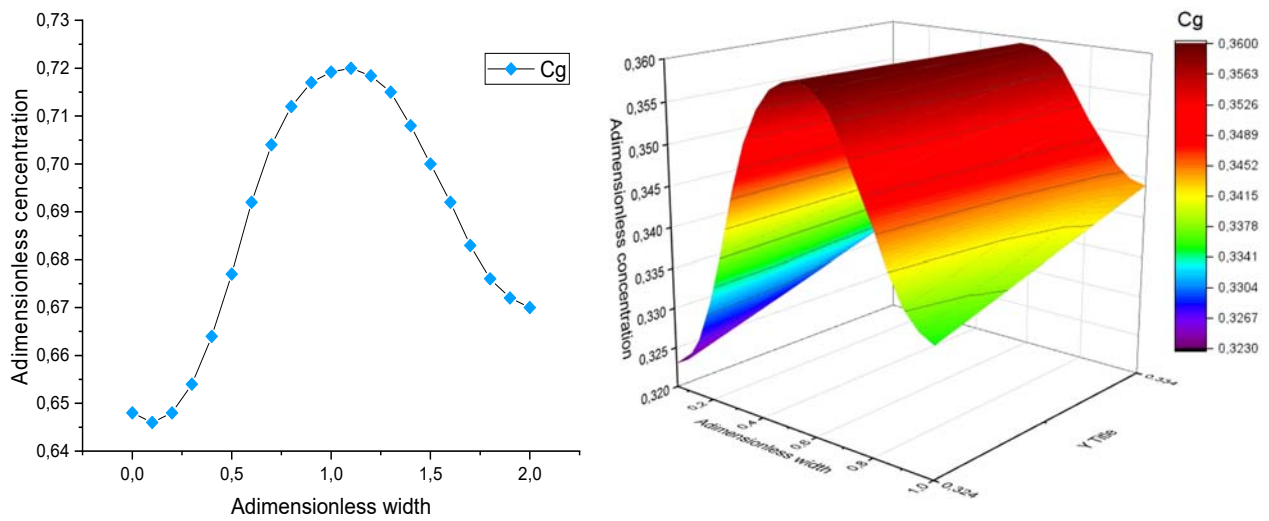


Fig.15. The dimensionless concentration of a granule Ti-6Al-4v as a function of dimensionless width.

Figures 14 and 15 show a variation in Ti-6Al-4v pellet concentration profiles as a function of width and time ($t = t/2, t = 3t/4, t = t/4$). It can be seen that the concentration of Ti-6Al-4v granules takes minimum values at the input and maximum values at the output. This result shows that the velocity of the fluid has an effect on the concentration and suspension of Ti-6Al-4v granules. [3], [5].

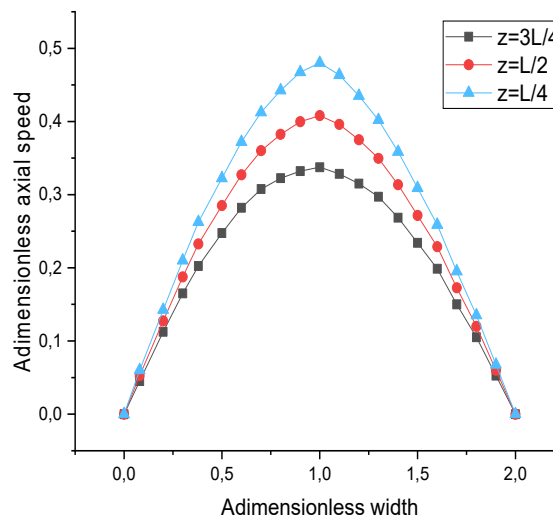


Fig.16. Axial velocity profile as a function of width.

Figures 16 and 17 show the variation of axial velocity as a function of width at three measures of length. An increase in length can be seen causing a decrease in the amplitudes of the axial velocity. This result shows that the pressure gradient is applied between the outlet and the inlet of the powder bed melt plate [3], [5], [20], [21].

Figure 19 shows the increase in the concentration of Ti-6Al-4v granules as a function of length. It can be said that at the entrance to the surface the concentration increases linearly as a function of length. This result is explained by the effect of fluid velocity on the suspension of Ti-6Al-4v granules.

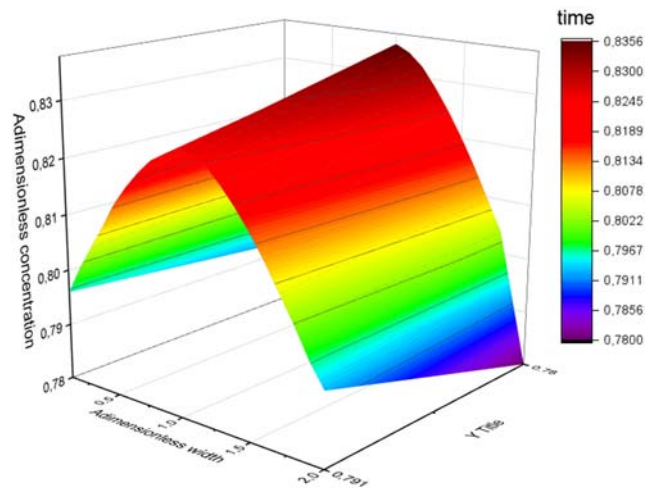
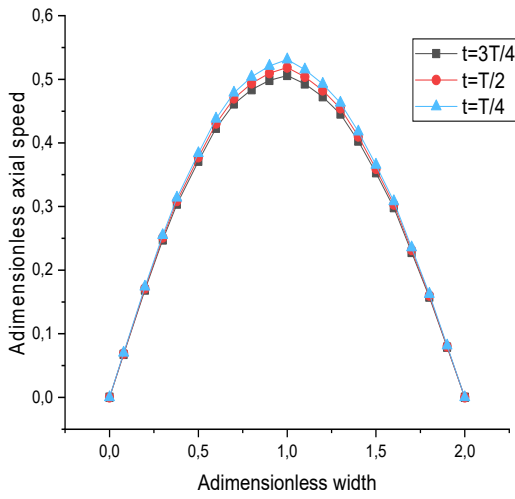


Fig.17. Profile of axial velocity as a function of width.

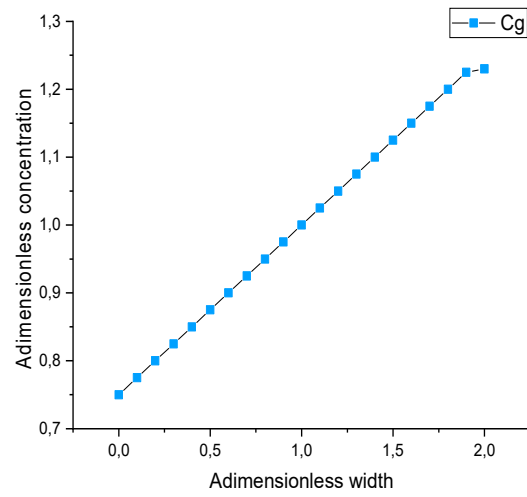
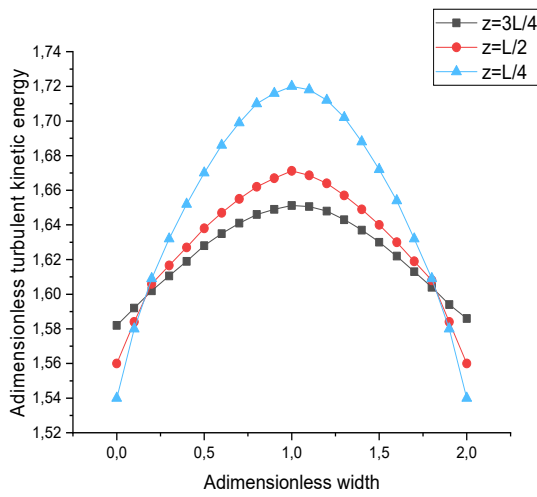


Fig.18. Turbulent kinetic energy profile.

Fig.19. Dimensionless granules Ti-6Al-4v concentration profile.

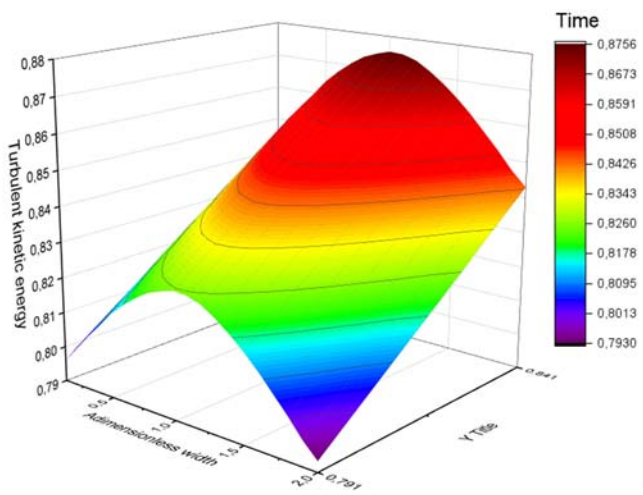
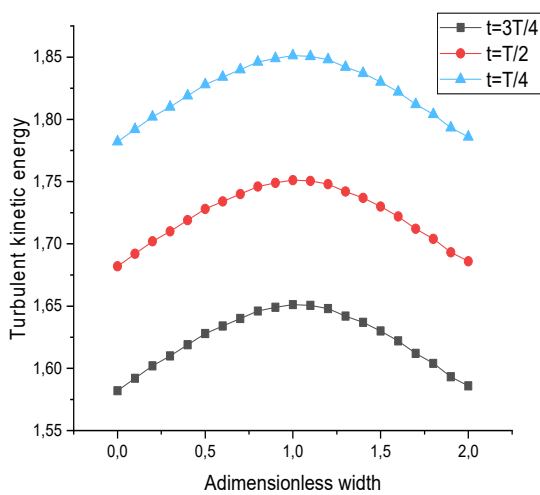


Fig.20. Turbulent kinetic energy profile.

Figures 18 and 20 illustrate that the turbulent kinetic energy varies with the three length values and with time. It can be seen that the profile of turbulent kinetic energy is a function of the velocity of the fluid, this result can be explained by the proportionality theorem between the turbulent kinetic energy and the velocity of the fluid [3], [5], [20], [21].

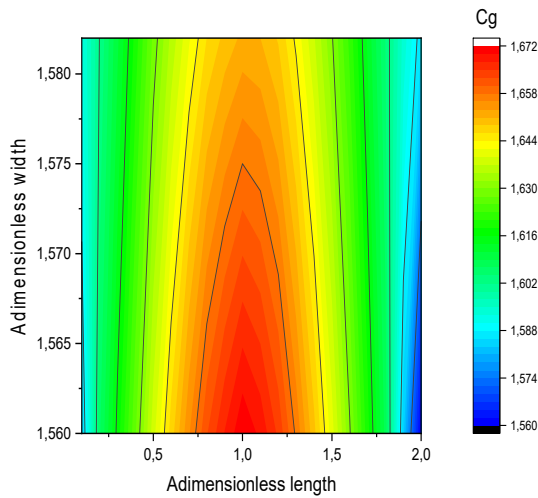


Fig.21. Granule concentration field

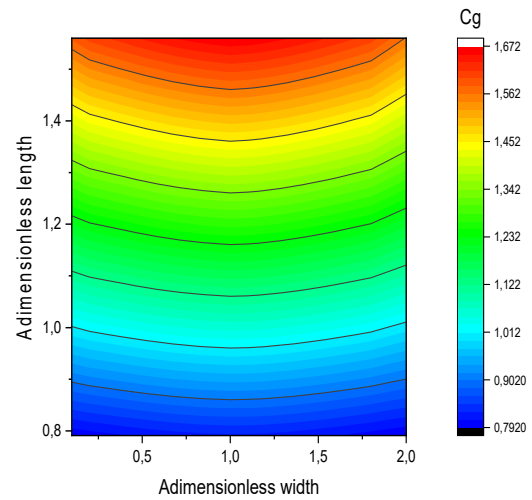


Fig.22. Granule of Ti-6Al-4v concentration field.

Figures 21 and 22 show the concentration field of Ti-6Al-4v granules after the onset of flow, it can be seen that at the entrance of the plate the concentration of granules increases with length. This result shows the influence of fluid velocity on the suspension of Ti-6Al-4v granules [3], [5], [20], [21].

6. Conclusion

We started with extreme approaches where we assumed the formation of a plasma as a result of the energy supply of the laser to the powder. Then, to check the presence or not of this plasma over the area optical analysis was performed using an emission spectrometer, Finally, a device was made with the aim of analyzing the particles present in metal vapor. In our study, we presented the results of the modeling of the transport process of Ti-6Al-4V granules in air streams. The equations of this process are solved in two-dimensional geometry. The results we obtained are similar to those of other authors who deal with the same phenomenon.

Acknowledgment

The sincere contribution of the research Team of Semiconductors and Sensor Technology for the Environment, Faculty of Science and Mohammed V University are sincerely appreciated by the authors.

Nomenclature

- C_g – granule concentration
- M_m – mass of molecular
- α, β – velocity components
- δ_c – number of Schmidt
- δ_e – remi-empirical coefficient
- κ_r – rate of dissipation of the turbulent kinetic energy

- κ_t – energy kinetic turbulent
 μ_M – dynamic viscosity
 τ_{C_g} – coefficient of concentration distribution granule
 Ψ – step at the moment t in space
 ν_f – viscosity of fluid kinematic
 ϕ_g – granule diameter

References

- [1] Mahboub M., Gueraoui K., Taibi M., Aberdane I., Kifani-Sahban F., Men-La-Yakhaf S. and El Marouani M. (2018): *Thermal treatment of Morocco sugarcane bagasse under inert atmosphere.*– International Review of Mechanical Engineering, vol.12, No.10, pp.860-868.
- [2] El Kailhal A., Gueraoui K., Mahboub M., Men-La-Yakhaf S., Taibi M., Kifani-Sahban F., Tagne M.S. (2021): *Mathematical and numerical modeling of algal oils transesterification.*– International Journal on Engineering Applications, vol.9, No.4, p.190, DOI:10.15866/irea.v9i4.19181.
- [3] Echchikhi A., Gueraoui K., El Houssaine El Rhaleb, Kifani-Sahban F., Benbih H. and Bounouar A. (2020): *Thermal treatments of wood (eucalyptus and maritime pin): experimental and theoretical study with chemical characterization.*– International Journal on Engineering Applications, vol.8, No.6, p.223, DOI:10.15866/irea.v8i6.19070.
- [4] Nasla S., Gueraoui K., Cherraj M., Jamil Y. and Bougtaib K. (2021): *Technical studies of Adobe bricks stabilize with lime from the quarry of the commune of Had Laghoualem in Morocco.*– International Journal on Engineering Applications (IREA), vol.9, No.1, DOI: <https://doi.org/10.15866/irea.v9i1.18791>.
- [5] Gueraoui K., Taibi M., Ghouli A., Mrabti A., Zeggwagh G. and Haddad Y. (2008): *Pulsating flow of inelastic fluids in anisotropic porous viscoelastic tubes.*– International Review of Mechanical Engineering, vol.2, pp.506-512.
- [6] Phillips M. (1980): *A force balance model for particle entrainment into a fluid stream.*– J. Phys. D: Appl. Phys., vol.13, pp.221-233.
- [7] Samrani H., Gueraoui K., Zeggwagh N.A., Taibi M. (2021): *Modeling of the impact of the geometric shape of a solar dryer on heat energy for different region in Morocco.*– International Journal on Engineering Applications, vol.9, No.2, DOI: <https://doi.org/10.15866/irea.v9i2.19180>.
- [8] Maftouh A., El Fatni O., Echchikhi A., Bahaj T., Gueraoui K. and El Houssaine El Rhaleb (2022): *Effect of feed water temperature on reverse osmosis performance in a borehole water desalination plant: numerical and experimental validation.*– International Journal on Engineering Applications, vol.10, No.4, DOI: <https://doi.org/10.15866/irea.v10i4.21290>.
- [9] El Hamma M., Rtibi A., Taibi M., Gueraoui K. and Bernatchou M. (2022): *Theoretical and numerical study of thermosolutal convection in a cylindrical porous cavity filled with a nanofluid and taking into account Soret and Dufour effects.*– International Journal on Engineering Applications, vol.10, No.1, DOI: <https://doi.org/10.15866/irea.v10i1.20809>.
- [10] Dirisu G.B., Okonkwo U.C., Okokpuije I.P. and Fayomi O.S. (2019): *Comparative analysis of the effectiveness of reverse osmosis and ultraviolet radiation of water treatment.*– Journal of Ecological Engineering, vol.20, No.1, pp.61-75.
- [11] Honarparvar S., Zhang X., Chen T., Alborzi A., Afroz K. and Reible D. (2021): *Frontiers of membrane desalination processes for brackish water treatment: a review.*– Membranes, vol.11, No.4., p.246.
- [12] Okampo E.J. and Nwulu N. (2021): *Optimization of renewable energy powered reverse osmosis desalination systems: a state-of-the-art review.*– Renewable and Sustainable Energy Reviews, vol.140, p.110712.
- [13] Filippini G., Al-Obaidi M.A., Manenti F. and Mujtaba I.M. (2019): *Design and economic evaluation of solar-powered hybrid multi effect and reverse osmosis system for seawater desalination.*– Desalination, vol.465, pp.114-125.
- [14] Sabbar J., Gueraoui K., Taibi M., Men-La-Yakhaf S. and Ouhimmou S. (2019): *Numerical solution of the pollutant's penetration in a specific soil in Tensift (South Morocco).*– International Review of Mechanical Engineering, vol.13, No.7, DOI: <https://doi.org/10.15866/ireme.v13i7.17030>.

- [15] Nchiti E., El Hammoumi A., Gueraoui K. and Iben Brahim A. (2020): *A comparative study of seismic and tsunami vulnerability of structures located in the coastal area of Rabat-Salé, Morocco.*– International Review of Mechanical Engineering, vol.14, No.4, DOI: <https://doi.org/10.15866/ireme.v14i4.18159>.
- [16] Belgada R., Gueraoui K., Mzerd A., Bellahkim M. and Benbih H. (2020): *A biological degradation model of sunflower waste with comparison of the growth profiles of microorganisms between the meal and the complete sunflower seed.*– International Journal on Engineering Applications, vol.8, No.3, DOI: <https://doi.org/10.15866/irea.v8i3.18579>.
- [17] Belgada R., Gueraoui K., Mzerd A., Taibi M., Ouhimmou S. and Benbih H. (2019): *Mathematical and numerical modeling of energy recovery of sunflower waste.*– International Journal on Engineering Applications, vol.7, No.5, DOI: <https://doi.org/10.15866/irea.v7i5.17707>.
- [18] Belarouf S., Samaouali A., Gueraoui K. and Rahier H. (2020): *Mechanical properties of concrete with recycled concrete aggregates.*– International Review of Civil Engineering, vol.11, No.6, DOI: <https://doi.org/10.15866/irece.v11i6.18478>
- [19] Zhang B., Liao H. and Coddet Ch. (2013): *Selective laser melting commercially pure Ti under vacuum.*– Vacuum, vol.95, pp.25-29, doi:10.1016/j.vacuum.2013.02.003.
- [20] Reid R.C., Prausnitz J.M. and Poling B.E. (1987): *The Properties of Gases and Liquids.*– Mc Graw Hill, p.507.
- [21] Hirschfelder J.O., Curtiss C.F. and Bird R.B. (1954): *Molecular Theory of Gases and Liquids.*– Wiley, pp.1110-1112.

Received: May 4, 2024

Revised: July 5, 2024